ECS Transactions, 35 (3) 111-120 (2011)
10.1149/1.3569904 ©The Electrochemical Society

Flexible Memristors Fabricated through Sol-Gel Hydrolysis [1]

J.L. Tedesco[†], N. Gergel-Hackett[†,2], L. Stephey[†,3], A.A. Herzing[‡], M. Hernández-Mora[†], J.J. Kopanski[†], C.A. Hacker[†], and C.A. Richter[†]

[†] National Institute of Standards & Technology, Semiconductor Electronics Division, 100 Bureau Drive, Gaithersburg, MD 20899, USA
[‡] National Institute of Standards & Technology, Surface and Microanalysis Science Division, 100 Bureau Drive, Gaithersburg, MD 20899, USA

Flexible memristors consisting of an oxide film generated through hydrolysis of a spun-on sol-gel were fabricated on polyethylene terephthalate substrates. X-ray photoelectron spectroscopy, spectroscopic ellipsometry, transmission electron microscopy, and electron energy loss spectroscopy measurements indicated that the oxide films contained amorphous TiO_2 as well as a significant fraction of organic material. This characterization indicated that the oxide film has a different structure and morphology than sputter-deposited TiO_2 memristors ("traditional memristors"). Despite the structural differences between sol-gel and traditional memristors, these flexible memristors exhibit switching behavior that is similar to sputter-deposited devices. Current-voltage (I-V) measurements suggest that this switching is not directly due to the electric field in the memristors. Additionally, thermal imaging measurements and I-V measurements performed after sectioning the memristors suggest that conduction occurred via localized conduction pathways. Capacitance-frequency and conductance-frequency measurements were also performed to further investigate conduction and loss mechanisms in these memristors.

Introduction

In 1971, Leon Chua theorized that, in addition to the resistor, capacitor, and inductor, there was a fourth fundamental two-terminal circuit element, which he called the "memristor" (1). This theory was based on an examination of the relationships between current, voltage, charge, and flux. Chua postulated that the memristor was a non-linear element and was, in fact, actually a subset of a larger class of dynamical devices known as memristive systems (2). At that time, a physical realization of the theoretical memristor had not been found, and the memristor was essentially forgotten.

In 2008, a team at HP Labs reported the first intentional fabrication of a memristor in a nanoscale Pt-TiO_2-Pt crossbar structure as well as an analytical model for

[1] Official contribution of the National Institute of Standards & Technology; not subject to copyright in the United States.
[2] Currently with the Department of Chemistry and Physics, Mary Baldwin College, Staunton, VA 24402, USA.
[3] Participated as a Society of Physics Students Summer Intern and is currently with the Department of Electrical & Computer Engineering, University of Wisconsin-Madison, Madison, WI 53706, USA.

Downloaded 06 May 2011 to 129.6.65.47. Redistribution subject to ECS license or copyright; see http://www.ecsdl.org/terms_use.jsp

its operation (3). Over the next two years, the HP team published a series of papers expanding on the properties of their memristors (4-9). While switching in TiO_2 was first reported in 1968 (10), and polarity-dependent switching in TiO_2-based devices has been studied by numerous researchers (11-20), the realization that the switching was evidence of memristance and a possible physical model explaining it (3,6) were the primary contributions of the HP team (5,22).

Memristor research has exploded since 2008 because their properties extend beyond the ability to act as a nonvolatile switch. It is also possible to switch the memristor between more than two states (3,23-24), enabling the memristor to be used in analog electronics. Furthermore, memristors could be used in logic schemes that would be inefficient for standard silicon-based electronics (25-26). These properties, along with low power requirements (27), mean that memristors could form the foundation of neuromorphic architectures (24) and enable computers to mimic the brain functionality of living creatures (24,27).

While the first memristors were fabricated on silicon (3), recently, memristors (and similar metal oxide-based devices referred to as nonvolatile bipolar resistive switching devices) have also been fabricated on flexible substrates (18-21,28-30). Flexible memristors would enable the integration of memristors with other flexible electronics. However, a greater understanding of the electrical characteristics of flexible memristors is necessary before they can be properly utilized. As a step toward gaining this understanding, flexible memristors were fabricated through hydrolysis of sol-gel on plastic substrates. The physical properties of these memristors were extensively characterized to determine their structure and morphology. They were also electrically characterized to begin to elucidate their switching and conduction properties.

Experimental Procedure

The flexible memristors used in this study were fabricated on the same polyethylene terephthalate (PET) substrates as reported previously (20). Stainless steel shadowmasks were mounted directly on PET substrates prior to loading them into a thermal evaporator. Aluminum (nominally 80 nm thick) was deposited in high vacuum conditions to form the bottom contact. Samples were then removed from the evaporator and a sol-gel was spun cast on to the entire sample (contact and substrate) in an argon glove box using the same parameters as previously reported (20). The sol-gel used was prepared from titanium(IV) isopropoxide (Sigma-Aldrich, 99.999 %) (31), 2-methoxyethanol (Sigma-Aldrich, ≥99.9 %), and ethanolamine (Sigma-Aldrich, 99+ %), by using a previously reported recipe (32). Some samples were prepared from a sol-gel dilution, where the original sol-gel was diluted by the addition of varying amounts of anhydrous ethanol (Sigma-Aldrich, 99.5+ %). Regardless of the sol-gel dilution used, after spinning, the samples were removed from the glove box and were left in ambient conditions for at least 1 h (more typically $\geq$ 24 h) to hydrolyze and form the oxide switching layer. During hydrolysis, samples were partially covered to ensure that particulates did not fall on them, but were otherwise left exposed to the air. Following hydrolysis, samples were loaded into the evaporator with a second shadowmask to evaporate the top contact. This contact was also aluminum and was the same thickness as the bottom contact. Memristors were fabricated with active regions of two sizes: 2 mm ×

Downloaded 06 May 2011 to 129.6.65.47. Redistribution subject to ECS license or copyright; see http://www.ecsdl.org/terms_use.jsp

2 mm (“large area memristors”) and 100 μm × 100 μm (“small area memristors”).

In order to understand the physical properties of the oxide films that were created during hydrolysis, they were analyzed by using an extensive suite of measurement techniques. X-ray photoelectron spectroscopy (XPS), Fourier transform infrared (FTIR) spectroscopy, and electron energy loss spectroscopy (EELS) were used to analyze the chemical characteristics of the oxide films. Variable angle spectroscopic ellipsometry (VASE) and transmission electron microscopy (TEM) measurements were used to assess the structural and morphological characteristics of the films. Optical profilometry and tapping mode atomic force microscopy (AFM) were also used to measure the morphology of the oxide films. The samples used for XPS, FTIR, VASE, AFM, and optical profilometry measurements were fabricated on silicon substrates. Oxide films for TEM and EELS measurements were spun on to amorphous lacey carbon films supported by copper TEM grids.

The electrical device behavior of the completed devices was characterized by current-voltage (I-V), capacitance-voltage (C-V), capacitance-frequency (C-f), and conductance-frequency (G-f) measurements, which were performed on the flexible memristors at room temperature in a probe station. During I-V measurements, the applied bias was ramped from zero to a particular value and back. This value was steadily increased to a maximum value of 10 V and 40 V for large area and small area memristors, respectively, until the memristor switched to the on-state. This process was then repeated with a negative bias until the memristor switched back to the off-state. The C-f and G-f measurements were performed at an applied bias of +1 V over a frequency range of 20 Hz to 2 MHz.

Results and Discussion

The XPS, FTIR, EELS, and VASE measurements of the oxide films formed through hydrolysis all confirmed that TiO_2 was formed in the hydrolyzed films. The XPS spectra also indicated that the films contained an excess of carbon as well as trace amounts of nitrogen and sodium. An example spectrum is shown in Fig. 1, which was recorded from an oxide film formed from sol-gel that had not been further diluted with ethanol. The carbon and nitrogen were assumed to be left over from the organic components of the sol-gel. Analysis of the XPS spectra suggested that the carbon content of these TiO_2 films was ≈ 50 %. The origin of the sodium shown in the spectrum is unknown. Electron energy loss spectroscopy measurements were also analyzed to determine the approximate elemental content of the films. However, the EELS measurements were acquired from samples formed from dilute sol-gel (10:1 and 80:1 dilutions). For the less dilute mixture, the EELS measurements showed comparable amounts of carbon and titanium. For the more dilute mixture, the amount of carbon was significantly elevated, which is reasonable given that the amount of solvent was significantly greater. However, the large local electron currents used during the EELS measurement can cause carbon migration that may lead to artificially large values for the carbon concentration. Dilution of the sol-gels did lead to controllable differences in the thickness of the TiO_2 films, as confirmed by VASE measurements. The thicknesses of the films were averaged from measurements of at least two separate samples and are shown in Table I. The standard deviations shown in Table I derive from these averages and

Downloaded 06 May 2011 to 129.6.65.47. Redistribution subject to ECS license or copyright; see http://www.ecsdl.org/terms_use.jsp

represent one standard deviation. Individual VASE measurements all had uncertainties less than 0.1 %. The FTIR, VASE, and TEM measurements indicated that the TiO_2 films, whether formed from diluted or undiluted sol-gel, were amorphous. Diffraction patterns of the TiO_2 films obtained by using the TEM are shown in Fig. 2. Figures 2(a) and 2(b) show the diffuse rings recorded from a 48 nm thick TiO_2 film and 17 nm thick TiO_2 film, respectively. These images were recorded from films that were suspended over holes in the lacey carbon support and thus showed no contribution from the underlying amorphous film. Figure 2(c) shows a diffraction pattern from a portion of the 48 nm thick TiO_2 film directly above the carbon support. The fact that the diffraction pattern is more defined in Fig. 2(c) indicates that the TiO_2 films alone are highly disordered. It is possible that a TiO_2 film consisting of sub-2 nm crystalline regions would produce diffraction patterns similar to those presented in Fig. 2. However, this seems unlikely given that the dielectric function from the VASE spectra (not shown) does not conform to that expected for a crystalline TiO_2 film and it is more likely that the films are amorphous.

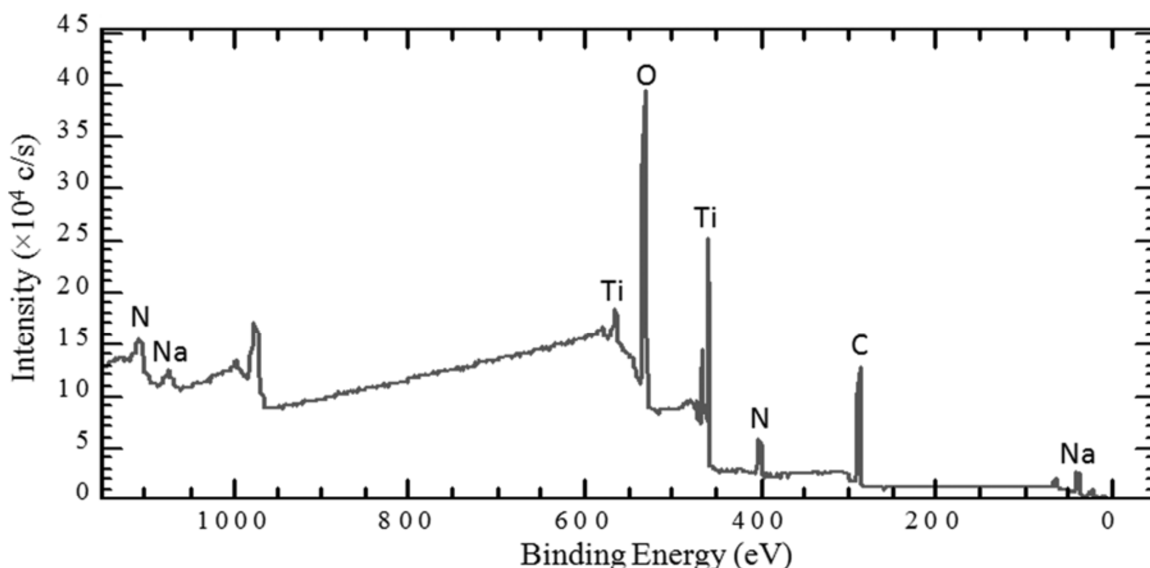

Fig. 1. XPS spectrum recorded from a 60 nm thick TiO_2 film.

TABLE I. The thickness of samples as measured by VASE depending on the dilution of the original sol-gel. The standard deviations in the thicknesses shown below are due to the averaging of several samples. The thickness of the undiluted film is taken from Gergel-Hackett et al. (23) where no standard deviation was provided.

Dilution ($mL_{ethanol}$:$mL_{sol-gel}$)	**Thickness (nm)**
Undiluted	60 [from (23)]
10:1	48.4 ± 2.8
20:1	33.1 ± 0.8
40:1	17.1 ± 1.1
80:1	8.5 ± 0.3

Transmission electron microscopy measurements indicate that there are domains containing titanium and oxygen surrounded by a carbon. This inhomogeneous nature of the TiO_2 films leads to an inhomogeneous surface morphology, which is likely due to actual differences in the thickness of the films. As shown in Fig. 3, there are significant differences in the surface roughness of the devices. These differences are present in

Downloaded 06 May 2011 to 129.6.65.47. Redistribution subject to ECS license or copyright; see http://www.ecsdl.org/terms_use.jsp

"thick" TiO_2 films (≈48 nm) as well as "thin" TiO_2 films (≈8 nm). Figure 3(a) shows an AFM image from a memristor with a 48 nm thick TiO_2 film while Fig. 3(b) shows an AFM image from a memristor with an 8 nm thick TiO_2 film. The height differences appear to be less pronounced in Fig. 3(b), likely due to the thinner film. Figure 3(c) shows an optical profilometry image recorded from a memristor with a thick TiO_2 film. The image was recorded at the edge of the active region. In the image, there is a visible difference in height between the active region and the adjacent contact; the inhomogeneities in the film morphology are not limited to the active region of the memristor. These inhomogeneities, however, are not the source of the differences in measured thickness shown in Table I because the VASE measurements were averaged over a spot size larger than the size of these morphological differences. To summarize the results of the analytical measurements, the inhomogeneities and the organic components of the TiO_2 films suggest that the structure of these sol-gel-based memristors is different than the structure of "traditional" TiO_2 memristors fabricated by using sputter deposition (3-4,7-9).

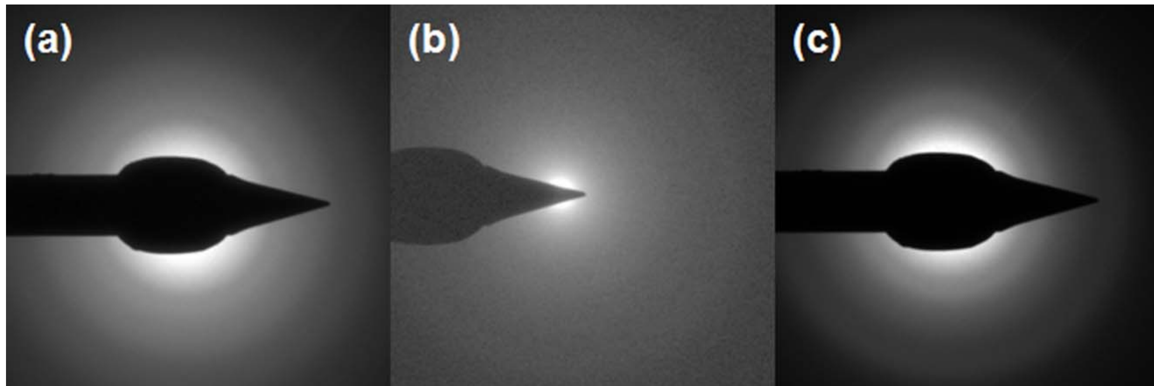

Fig. 2. Diffraction rings recorded during TEM measurements of (a) a 48 nm thick TiO_2 film and (b) a 17 nm thick TiO_2 film, both suspended over holes in the lacey carbon support. (c) Diffraction ring recorded from an area of the 48 nm thick film supported by the lacey carbon film.

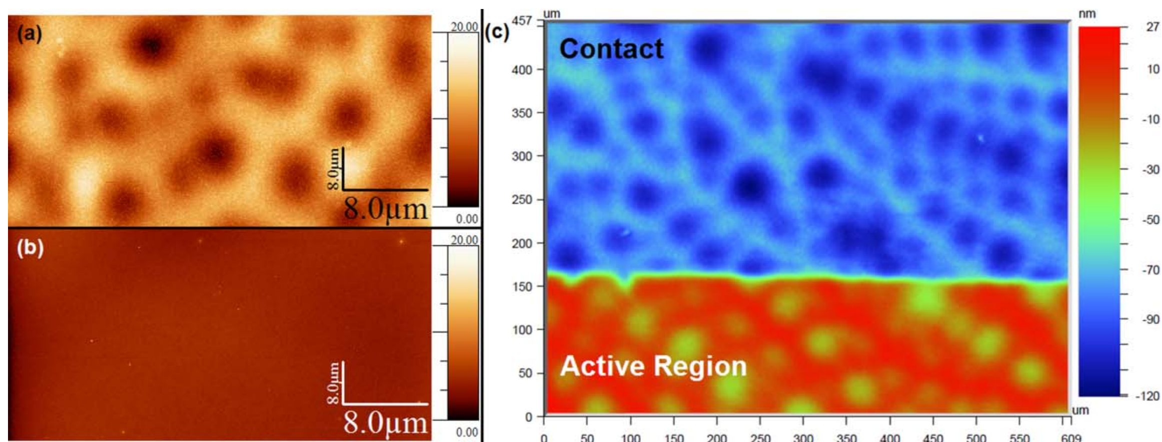

Fig. 3 (color online). AFM images of (a) a 48 nm thick TiO_2 film and (b) a 8 nm thick TiO_2 film. The height scales are in units of nanometers. (c) Optical profilometry image recorded along the edge of the active region of the memristor from (a). The region labeled "Active Region" refers to the Al/TiO_2/Al active region of the memristor, while the region labeled "Contact" refers to the top contact, which is aluminum on TiO_2.

Downloaded 06 May 2011 to 129.6.65.47. Redistribution subject to ECS license or copyright; see http://www.ecsdl.org/terms_use.jsp

While the structure of the oxide switching layer in these sol-gel memristors is different than the corresponding film in traditional memristors, their electrical behavior (illustrated in the inset to Fig. 4) is similar to traditional memristors. In an effort to better understand the source of the switching in the sol-gel-based memristors, devices were fabricated with two different areas, and the thickness of the TiO_2 film was varied. When different TiO_2 thicknesses and small area memristors are also considered, there is a difference in the switching characteristics of the large and small area memristors, as shown in Fig. 4. The large area memristors all switched at approximately the same applied bias, regardless of TiO_2 thickness. The small area memristors, however, exhibit a trend: the applied switching bias increases for TiO_2 thicknesses of 48 nm, but is essentially constant for thinner TiO_2 films. An example of an I-V curve from a small area memristor with an oxide thickness of 33 nm is shown in the inset of Fig. 4. These trends of switching bias with applied electric field are different than the expected trend if switching were directly induced by the electric field in the memristors. Were the electric field the direct cause of switching, the switching bias would increase proportionally with TiO_2 thickness (33). Therefore, while the switching could be explained by using a model based on the diffusion of mobile charged oxygen vacancies through the oxide (3,6,16,34), the driving force behind the motion of these vacancies is not directly proportional to the electric field. Therefore, further study is required to fully understand the electrical switching in these devices.

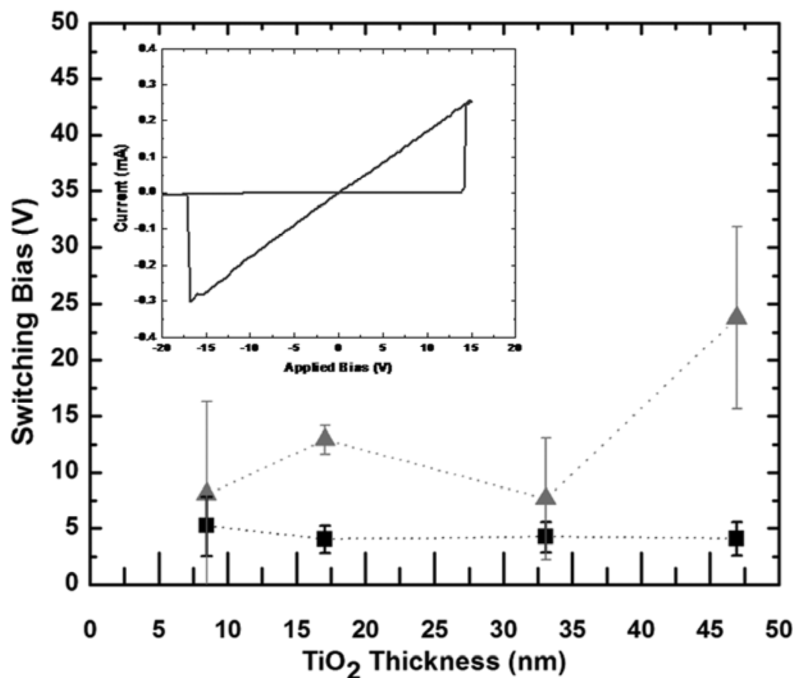

Fig. 4. Values of the bias required to switch large area memristors (■) and small area memristors (▲) based on the thickness of their TiO_2 film. The error bars represent one standard deviation. The inset shows an I-V curve from a small area memristor with a TiO_2 thickness of 33 nm.

In order to determine the origin of switching, flexible memristors in the on-state were cut into two halves. The I-V measurements were nearly identical to the original measurements for only one half, while the other half showed significantly lower current, suggesting that switching was due to at least one localized conductance channel. Similar results have been reported in studies on sectioned traditional memristors (4). In order to investigate the conduction channels in these sol-gel memristors, thermal imaging measurements were performed on the large area sol-gel memristors. Figure 5 shows a series of images of the active region of a large area memristor. Figure 5(a) shows an image recorded with an optical microscope prior to bias being applied. Figures 5(b)

Downloaded 06 May 2011 to 129.6.65.47. Redistribution subject to ECS license or copyright; see http://www.ecsdl.org/terms_use.jsp

through 5(d) show a progression of images as the bias applied to the memristor was increased. Eventually, as shown in Fig. 5(d), a single hot spot appeared, suggesting that there was one dominant conduction channel in the device. The hot spot reappeared upon repeated application of the bias. In order to more easily see the hot spot in Fig. 5(d), only the portion of the active region exhibiting the hot spot was shown in Fig. 5 (the rest of the active region was essentially featureless). A scanning transmission X-ray microscopy study of traditional memristors (the devices had active regions 2 μm × 3 μm in size) also showed that only one conducting channel was formed within the active region (9).

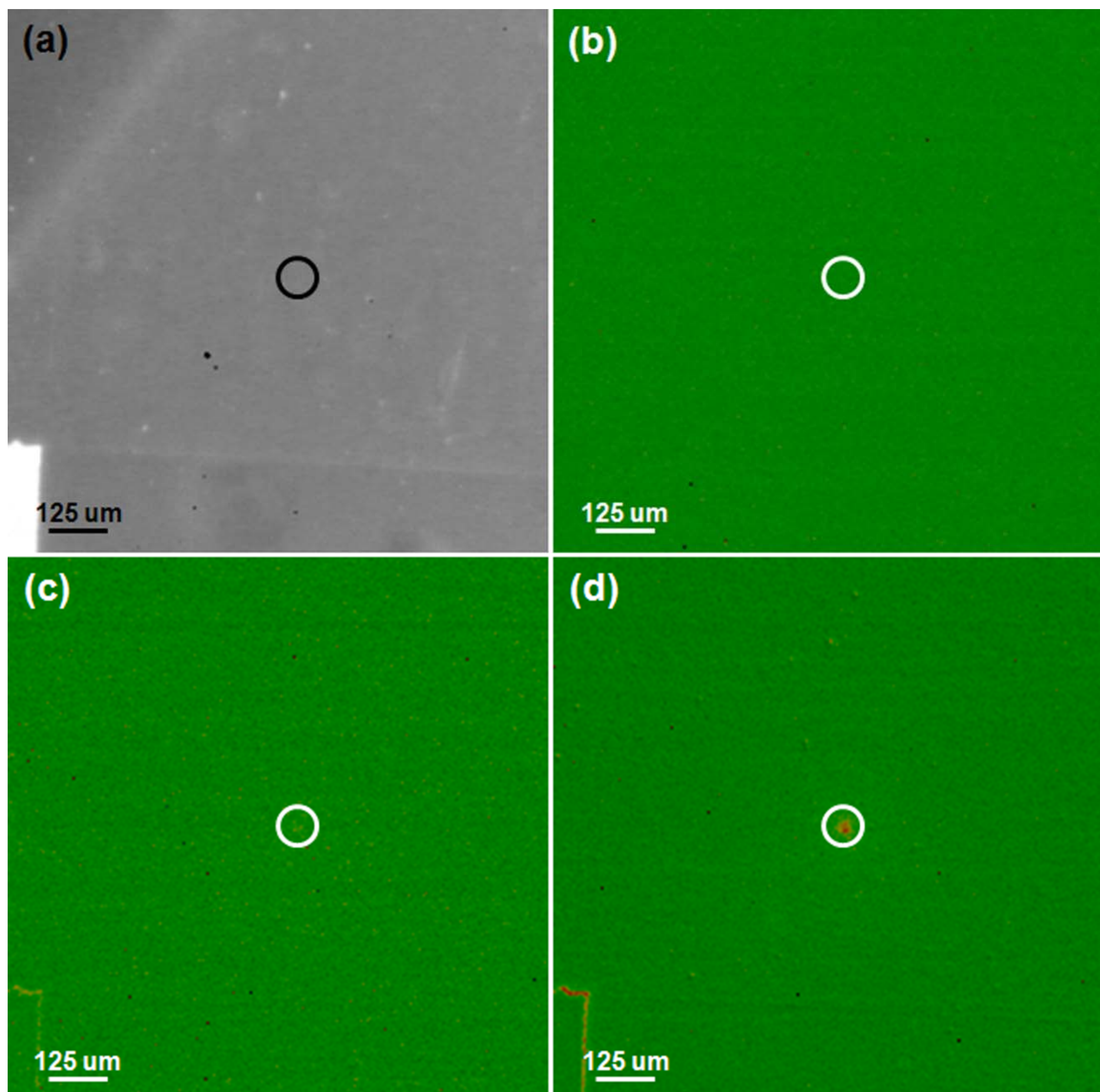

Fig. 5 (color online). (a) Optical microscopy image of part of the active region of a large area memristor. Thermal images recorded at a constant applied bias of (b) +10 V, (c) +15 V, and (d) +20 V. The location of the hot spot is circled in all four images.

To further study the charge conduction within the memristors, capacitance measurements were performed at room temperature. The memristors were first put into either the on-state or off-state prior to performing the capacitance measurements. It was confirmed that the devices were still in the same state following the capacitance measurements. The C-V curves (not shown) show no significant voltage dependence

Downloaded 06 May 2011 to 129.6.65.47. Redistribution subject to ECS license or copyright; see http://www.ecsdl.org/terms_use.jsp

regardless of the state of the memristors. The C-f and G-f curves (not shown) do exhibit differences between the on-state and off-state. Both the on-state and off-state have a roll-off in the capacitance (and an accompanying increase in conductance) for frequencies above ≈20 kHz that is attributed to dielectric loss mechanisms due to the organic components in the TiO_2 films. This is a reasonable conclusion given that a study of deposited TiO_2 films showed admittance-frequency (the real part of the admittance is equal to the conductance) curves that do not exhibit such effects (12). Furthermore, a previous study of $SrZiO_3$ that was also prepared by using sol-gel methods showed similar effects at high frequency (35). Additionally, in the memristors in this study, there is also a peak at ≈1 GHz observed for the off-state device (but not for the on-state) in these measurements that indicates an additional dielectric loss mechanism was present prior to switching to the higher current state. Ultimately, a complete investigation is necessary to fully elucidate the dielectric loss mechanisms as well as the distribution of charge traps within the TiO_2 films.

Summary

Flexible memristors composed of TiO_2 films formed through sol-gel hydrolysis were fabricated on PET substrates. While the electrical behavior of these memristors was found to be similar to traditional memristors, extensive analytical characterization of the TiO_2 layers indicates that the films are amorphous with nonhomogeneous surface morphologies and contain, in some cases, significant quantities of impurities. Experiments in which memristors were cut into two pieces showed that only one piece retained the I-V characteristics of the original memristor upon subsequent measurements. This result suggests that switching is due to conduction through localized conductance channels. Thermal imaging measurements support this conclusion. Capacitance and conductance measurements showed that there was a difference in the conduction mechanism depending on whether the memristor was in the off-state or the on-state.

Acknowledgements

This research was supported in part by the Office of Microelectronics Programs. J.L.T. acknowledges the IC Postdoctoral Research Fellowship Program and L.S. acknowledges the APS Society of Physics Students Summer Internship Program. The authors also acknowledge L.J. Richter for assistance with the VASE measurements and helpful discussions and R.A. Allen for assistance with the optical profilometry measurements.

References

1. L.O. Chua, *IEEE Trans. Circ. Theory*, **18**, 507 (1971).
2. L.O. Chua and S.M. Kang, *Proc. IEEE*, **64**, 209 (1976).
3. D.B. Strukov, G.S. Snider, D.R. Stewart, and R.S. Williams, *Nature*, **438**, 80 (2008).
4. J.J. Yang, M.D. Pickett, X. Li, D.A.A. Ohlberg, D.R. Stewart, and R.S. Williams, *Nature Nanotech*., **3**, 429 (2008).
5. R.S. Williams, *IEEE Spectr*., **45(12)**, 29, (2008).

Downloaded 06 May 2011 to 129.6.65.47. Redistribution subject to ECS license or copyright; see http://www.ecsdl.org/terms_use.jsp

6. D.B. Strukov, J.L. Borghetti, and R.S. Williams, *Small*, **5**, 1058 (2009).
7. M.D. Pickett, D.B. Strukov, J.L. Borghetti, J.J. Yang, G.S. Snider, D.R. Stewart, and R.S. Williams, *J. Appl. Phys.*, **106**, 074508 (2009).
8. J. Borghetti, D.B. Strukov, M.D. Pickett, J.J. Yang, D.R. Stewart, and R.S. Williams, *J. Appl. Phys.*, **106**, 124504 (2009).
9. J.P. Strachan, M.D. Pickett, J.J. Yang, S. Aloni, A.L.D. Kilcoyne, G. Medeiros-Ribeiro, and R.S. Williams, *Adv. Mater.*, **22**, 3573 (2010).
10. F. Argall, *Solid-State Electron.*, **11**, 535 (1968).
11. B.J. Choi, D.S. Jeong, S.K. Kim, C. Rohde, S. Choi, J.H. Oh, H.J. Kim, C.S. Hwang, K. Szot, R. Waser, B. Reichenberg, and S. Tiedke, *J. Appl. Phys.*, **98**, 033715 (2005).
12. D.S. Jeong, H. Schroeder, and R. Waser, *Appl. Phys. Lett.*, **89**, 082909 (2006).
13. D.S. Jeong, H. Shroeder, and R. Waser, *Electrochem. Solid-State Lett.*, **10**, G51 (2007).
14. L.-E. Yu, S. Kim, M.-K. Ryu, S.-Y. Choi, and Y.-K. Choi, *IEEE Electron Device Lett.*, **29**, 331 (2008).
15. R. Waser, R. Dittman, G. Staikov, and K. Szot, *Adv. Mater.*, **21**, 2632 (2009).
16. H.Y. Jeong, J.Y. Lee, S.-Y. Choi, and J.W. Kim, *Appl. Phys. Lett.*, **95**, 162108 (2009).
17. H.Y. Jeong, J.Y. Lee, M.-K. Ryu, and S.-Y. Choi, *Phys. Status Solidi RRL*, **4**, 28 (2010).
18. S. Kim, O. Yarimaga, S. Choi, and Y. Choi, *Solid-State Electron.*, **54**, 392 (2010).
19. H.Y. Jeong, Y.I. Kim, J.Y. Lee, and S.-Y. Choi, *Nanotechnology*, **21**, 115203 (2010).
20. M.H. Lee, K.M. Kim, G.H. Kim, J.Y. Seok, S.J. Song, J.H. Yoon, and C.S. Hwang, *Appl. Phys. Lett.*, **96**, 152909 (2010).
21. H.Y. Jeong , J.Y. Lee , and S.-Y. Choi, *Adv. Funct. Mater.*, **20**, 3912 (2010).
22. R.S. Williams, *IETE Tech. Rev.* **27**, 181 (2010).
23. N. Gergel-Hackett, B. Hamadani, B. Dunlap, J. Suehle, C. Richter, C. Hacker, and D. Gundlach, *IEEE Electron Device Lett.*, **30**, 706 (2009).
24. S.H. Jo, T. Chang, I. Ebong, B.B. Bhadviya, P. Mazumdar, and W. Lu, *Nano Lett.*, **10**, 1297 (2010).
25. Q. Xia, W. Robinett, M.W. Cumbie, N. Banerjee, T.J. Cardinali, J.J. Yang, W. Wu, X. Li, W.M. Tong, D.B. Strukov, G.S. Snider, G. Medeiros-Ribeiro, and R.S. Williams, *Nano Lett.*, **9**, 3640 (2009).
26. J. Borghetti, G.S. Snider, P.J. Kuekes, J.J. Yang, D.R. Stewart, and R.S. Williams, *Nature*, **464**, 873 (2010).
27. M. Versace and B. Chandler**,** *IEEE Spectr.*, **47(12)**, 30 (2010).
28. S. Lee, H. Kim, D.-J. Yun, S-W. Rhee, and K. Yong, *Appl. Phys. Lett.*, **95**, 262113 (2009).
29. S.K. Hong, J.E. Kim, S.O. Kim, S.-Y. Choi, and B.J. Cho, *IEEE Electron Device Lett.*, **31**, 1005 (2010).
30. H.Y. Jeong, J.Y. Kim, J.W. Kim, J.O. Hwang, J.-E. Kim, J.Y. Lee, T.H. Yoon, B.J. Cho, S.O. Kim, R.S. Ruoff, and S.-Y. Choi, *Nano Lett.*, **10**, 4381 (2010).
31. Certain equipment, instruments, or materials are identified in this paper in order to adequately specify the experimental details. Such identification neither implies recommendation by the National Institute of Standards and Technology nor does it imply the materials are necessarily the best available for the purpose.
32. J.Y. Kim, S.H. Kim, H.-H. Lee, K. Lee, W. Ma, X. Gong, and A.J. Heeger, *Adv. Mater.*, **18**, 572 (2006).

Downloaded 06 May 2011 to 129.6.65.47. Redistribution subject to ECS license or copyright; see http://www.ecsdl.org/terms_use.jsp

33. $V_{switch} = E_{switch} \bullet d_{oxide}$, where E_{switch} is the electric field at the switching point, V_{switch} is the applied switching bias, and d_{oxide} is the thickness of the TiO_2 film. If E_{switch} is constant for a given switching oxide, $V_{switch} \propto d_{oxide}$. Referring to the data in Fig. 4, for example, if E_{switch} is determined from the devices with 17.1 nm thick TiO_2 films, for the memristors with 33 nm thick TiO_2 films the switching bias would then be 24.9 ± 2.5 V if the switching was directly caused by the electric field (significantly greater than the experimentally observed values of 7.7 ± 5.4 V).
34. B. Gao, B. Sun, H. Zhang, L. Liu, X. Liu, R. Han, J. Kang, and B. Yu, *IEEE Electron Device Lett*., **30**, 1326 (2009).
35. H.-Q. Ling, A.-D. Li, D. Wu, Y.-F. Tang, Z.-G. Liu, and N.-B. Ming, *Mater. Chem. Phys*., **75**, 170 (2002).

Downloaded 06 May 2011 to 129.6.65.47. Redistribution subject to ECS license or copyright; see http://www.ecsdl.org/terms_use.jsp